Flow Measurement and Instrumentation 57 (2017) 20–27

Contents lists available at ScienceDirect

Flow Measurement and Instrumentation

journal homepage: www.elsevier.com/locate/flowmeasinst

Algorithm with improved accuracy for real-time measurement of flow rate in open channel systems

Cornelius E. Agu[a,*], Åsmund Hjulstad[b], Geir Elseth[b], Bernt Lie[a]

[a] Faculty of Technology, University College of Southeast Norway, 3918 Porsgrunn, Norway
[b] Statoil ASA, Postboks 8500, 4035 Stavanger, Norway

ARTICLE INFO

Keywords:
Circular channel
Saint Venant equation
Non-Newtonian fluid
Venturi channel

ABSTRACT

Most methods for flow rate measurement in open channels usually have low accuracy over a range of flow rates due to varying fluid properties, flow conditions and channel length. This paper suggests an algorithm to improve on the accuracy of flow rates computed based on hydraulic structure and slope-hydraulic radius methods. A model for determining flow rates in accelerating flows is also developed. In the proposed algorithm, the parameter used for adapting the flow rate *models* is obtained by comparing the measured fluid depth with the depth simulated based on the one-dimensional Saint Venant equations. The results show that an improvement from ± 2.3% to ± 0.8% accuracy in the flow rate measurement using the Venturi flume method could be achieved. In unsteady state flow in a straight-run channel, the results based on flow simulation also show possibility of achieving accurate computation over a wide range of flow rates.

1. Introduction

Fluid flow in an open channel has many industrial applications. It is applied in transportation of slurries, water supply for irrigation, and river flow control [1]. In these fields, accurate flow measurements are important for proper flow distribution and control for safe operations. In open channels, the flow rate is usually difficult to measure directly. Most methods employed are based on computation of flow rate from measurements of other variables that can be measured directly. Such variables include channel width, channel depth, channel slope and channel velocity. Among other methods, the timed gravimetric, the area-velocity, the slope-hydraulic radius and the hydraulic structure methods are used for flow rate measurements in open channels [2].

The timed gravimetric method is limited to flow rates less than100 litres/min and is not suitable for continuous flow. The area-velocity method requires measurement of average velocity of the flow over a known cross-section. The area-velocity method uses pressure transducer and Doppler ultrasonic sensor for depth and velocity measurements, respectively. These instruments are sensitive to flow disturbances, thus resulting in error ± 10% in the measurement [3]. In the slope-hydraulic radius method, a flow resistance model such as the Manning formula is utilized. The method is applied in uniform flows, and is best suited for sizing open channels due to its simplicity. For control purpose, the slope-hydraulic radius method is not suitable due to its wide measurement error in the range of 25–30%. The measurement error is due to uncertainty in determining the correct frictional parameter, such as Manning's roughness coefficient that characterises the flow. Another common method is the use of hydraulic structures such as weirs and flumes. Both structures introduce a restriction in the flow direction, which leads to changes in the approach velocity and in the liquid depth in the channel. The measurement of flow rate with a flume or weir is based on the unique depth-flow rate relationship established in the flow by the structure. Although flumes and weirs show high accuracy (2–6%) under laboratory observations, the field accuracy still lies within ± 10% [4]. This is due to uncertainties in measurement of the level, and due to difficulties in obtaining the correct discharge coefficient for correction of losses in the theoretical depth-flow rate relationship.

This paper focuses on the use of hydraulic structures and slope-hydraulic radius measurement techniques, where the liquid depth is the only physical measurement required to compute the flow rate in a given channel geometry. These techniques are easier to manipulate in designing a software for flow control in open channels. Normally, the hydraulic structures (flumes or weirs) are installed in applications where the flow upstream is subcritical (that is, the flow condition where the flow velocity is less than the gravity wave celerity). When the velocity is greater than the wave speed (celerity), the flow condition is supercritical flow. At the transition between subcritical and supercritical conditions, the flow is critical, that is, the flow velocity and the wave speed are the same. In general, flumes are designed depending on

* Corresponding author.
E-mail addresses: cornelius.e.agu@usn.no (C.E. Agu), ahju@statoil.com (Å. Hjulstad), geiel@statoil.com (G. Elseth), bernt.lie@usn.no (B. Lie).

http://dx.doi.org/10.1016/j.flowmeasinst.2017.08.008
Received 18 April 2017; Received in revised form 1 August 2017; Accepted 9 August 2017
Available online 12 August 2017

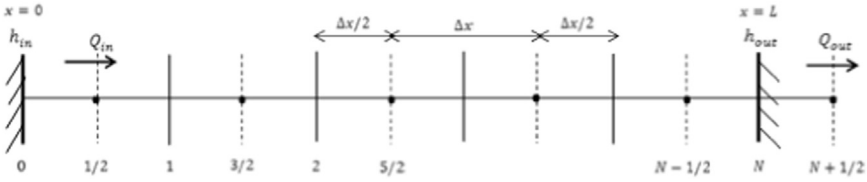

Fig. 1. Computation nodes for liquid depth and flow rate along the channel length.

whether the approaching fluid flow is subcritical or supercritical. Wilson [5] described the design of straight-run channels for measurement of flow rates in supercritical condition. Similar to subcritical Venturi flumes, Kilpatrick et al. [6] and Smith et al. [7] gave clear discussions on development of supercritical flumes. The problems with the use of supercritical Venturi flume are the difficulty to obtain critical flow conditions for all flow rates, and the possibility of deposition of fluid debris or suspensions. These challenges limit the measurement range as well as the hydraulic control of the flume. The slope-hydraulic radius method can be applied in supercritical flow conditions, but this will require in addition to uniform flow model, a model for accelerating flows, since the flow may not have reached a uniform flow before discharging the channel.

There are several studies and model reviews on flow rate measurement in open channels [8–10]. The possibility of estimating drilling mud flow rate for kick/loss detection using a Venturi channel flow rate model is discussed in Berg et al. [11], where it is shown that the required tuning parameter for the model depends on the fluid properties due to non-Newtonian behaviour of the fluid. In this paper, an algorithm is presented for computing flow rate in open channels with improved accuracy. The developed method could be suitable for software implementation in open channels in both subcritical and supercritical upstream flow conditions. The desired improved accuracy is obtained by continuous calibration of the model applied in each of the slope-hydraulic radius and hydraulic structure techniques. In order to achieve this, the flow through the channel is simulated using the estimated flow rate, and the simulated fluid depth is compared with the measured fluid depth. The difference in the simulated and measured depths is used to continuously adjust a tuning parameter in the flow rate model until the difference between the simulated and the measured depths is within a tolerance level.

The success of this algorithm depends on a suitable 1-D unsteady state model that can be applied to simulate the flow in an open channel. The Saint Venant equations have been long established as a good 1-D model that predicts the flow behaviour in an open channel. The accuracy and speed of execution of these hyperbolic partial differential equations depend on the numerical scheme employed. A number of numerical algorithms for solving the Saint Venant equations have been developed [12–14]. The simplified numerical scheme described in Agu et al. [15] for solving the nonlinear equations, is applied in this paper.

In the following sections, the governing equations are presented, and the iterative algorithm for computation of the flow rate using both the hydraulic structure and the slope-hydraulic radius methods, are described. Simulation results based on the algorithms are presented, and their accuracy and speed of execution are discussed. Finally, some conclusions are drawn.

2. Governing equation

The unsteady state flow of fluid in an open channel of any kind of cross section can be described by the one-dimensional Saint Venant equations [16]

$$\frac{\partial A}{\partial t} + \frac{\partial Q}{\partial x} = 0 \tag{1}$$

$$\frac{\partial Q}{\partial t} + \frac{\partial\left(\frac{\beta Q^2}{A}\right)}{\partial x} = gA(\sin\theta - S_f) - gA\cos\theta\frac{\partial h}{\partial x}. \tag{2}$$

Here, Q is the volumetric flow rate, and A and h are the flow cross sectional area and free surface liquid depth, respectively. θ is the channel angle of inclination, and g is the acceleration due to gravity. β is the momentum correction coefficient with a value between 1.03 and 1.07. x is the position along the channel axis and t is the time. For a Newtonian fluid, the frictional slope S_f is given by Manning's equation

$$S_f = (|V|n_M)^2 R_h^{-4/3}, \tag{3}$$

where n_M is the Manning's roughness coefficient, $V = Q/A$ is the average flow velocity and $R_h = \frac{A}{P_w}$ is the hydraulic radius, where P_w is the wetted perimeter at the flow cross section. In non-Newtonian fluid flows, the internal frictional shearing stresses dominate. Based on the velocity profile for a power law fluid rheology [17], S_f is obtained as given in Eq. (4). For yield-pseudo-plastic fluid rheology, S_f is given by Eq. (5) according to Jin and Fread [18].

$$S_f = \frac{K}{4\rho g R_h}\left(\frac{|V|}{h}\frac{1+2n}{n}\right)^n, \tag{4}$$

$$S_f = \frac{\tau_y}{\rho g R_h}\left[1+\left(\frac{(\epsilon+1)(\epsilon+2)|V|}{(0.74+0.656\epsilon)\left(\frac{\tau_y}{K}\right)^{\epsilon} R_h}\right)^{\frac{1}{\epsilon+0.15}}\right]. \tag{5}$$

Here, ρ, τ_y, K and n (or $\epsilon \equiv \frac{1}{n}$) are fluid properties denoting the density, yield shear stress, flow consistency coefficient and fluid behaviour index, respectively.

The numerical solution of Eqs. (1) and (2) can be obtained as in Agu et al. [15], with notation for the spatial discretization as given in Fig. 1, where the computation nodes for the liquid depth are at the cell centres ($i = 1,2,3,..,N$) and those for the flow rate are at the cell faces ($i = \frac{3}{2}, \frac{5}{2}, \frac{7}{2},..,N+\frac{1}{2}$) based on a staggered grid arrangement. Eqs. (6) and (7) describe the discretized forms of Eqs. (1) and (2).

$$\frac{dA_i}{dt} = -\frac{Q_{i+1/2} - Q_{i-1/2}}{\Delta x}, \tag{6}$$

$$\frac{dQ_{i+1/2}}{dt} = -\beta\frac{(QV)_{i+1} - (QV)_i}{\Delta x} - g\overline{A}_{i+1/2}\cos\theta\,\frac{h_{i+1} - h_i}{\Delta x} + g\overline{A}_{i+1/2}(\sin\theta - S_{fi+1/2}). \tag{7}$$

Applying the first order upwind scheme,

$$(QV)_i = \frac{Q_{i+1/2} + Q_{i-1/2}}{2}V_{i-1/2}$$

$$V_{i-1/2} = \frac{Q_{i-1/2}}{\overline{A}_{i-1/2}},$$

where $\overline{A}_{i+1/2}$ is the average cross sectional area for each cell face, and is calculated based on the average cell centre liquid depth, $\frac{h_{i+1}+h_i}{2}$

2.1. Boundary conditions and inputs

At the upstream boundary, the values of $h(t, x = 0)$ and $Q(t, x = 0)$ are designated as input corresponding to h_0 and $Q_{1/2}$, respectively, as shown in Fig. 1. The downstream boundaries are $h(t, x = L)$ and $Q(t, x = L)$ corresponding to h_N and $Q_{N+1/2}$, respectively. Normally,

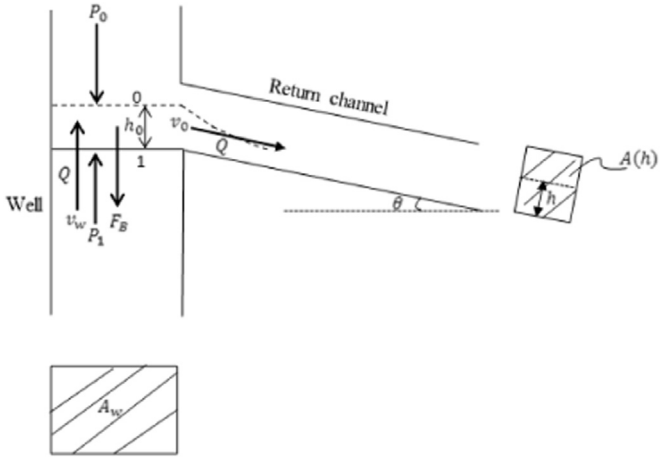

Fig. 2. Free body diagram for flow from a well into a return channel.

$Q(t, x = 0)$ is specified along with one of $h(t, x = 0)$ and $h(t, x = L)$ depending on the flow condition: for a pure subcritical flow, both upstream and downstream boundaries are specified with a combination of depth and flow rate. In a pure supercritical flow, only the upstream boundary is specified with the flow variables $h(t, x = 0)$ and $Q(t, x = 0)$. When the flow transits from subcritical upstream to supercritical downstream as in free-flowing flumes and weirs, only the upstream flow rate is used to determine the flow behaviour. The necessary boundary equation for a given boundary input is also described in Agu et al. [15].

One of the challenges in simulating supercritical flows is obtaining accurate measurement of the input liquid depth, owing to the dynamic nature of the upstream boundary due to disturbances and due to the flow being under development. In most practical flows, such as that from a well into an open channel diverter, an estimation of input depth can be obtained by applying momentum and energy balances over the fluid volume discharging from the well. Neglecting internal fluid resistance and wall interaction effect within the displaced liquid volume shown in Fig. 2, the steady state momentum balance across the fluid volume in the vertical direction can be expressed as

$$-\rho Q v_0 sin\theta - \rho Q v_w = (P_1 - P_0)A_w - F_B, \tag{8}$$

where $F_B = \rho g A_w h_0$ is the weight of fluid volume, v_0 is the entry velocity of fluid into the return channel, v_w is the flow velocity of fluid within the well at a given flow rate, A_w is the flow cross-sectional area of the well, and h_0 is the liquid depth at the entrance to the channel where A_0 is the corresponding flow area.

Applying Bernoulli's principle for energy balance over the fluid volume, neglecting energy losses,

$$\frac{P_1}{\rho g} + \frac{{v_w}^2}{2g} + h_p = \frac{P_0}{\rho g} + \frac{{v_0}^2}{2g} + h_0.$$

Here, h_p is the energy per unit weight contributed by a pump to overcome the potential energy due to fluid level as well as the internal losses within the fluid volume. Assuming that the pump energy is just sufficient to overcome the fluid potential energy,

$h_0 - h_p = 0$, leading to

$$P_1 - P_0 = \frac{\rho}{2}({v_0}^2 - {v_w}^2). \tag{9}$$

Substituting (9) into (8),

$$-\rho Q v_0 sin\theta - \rho Q v_w = \frac{\rho A_w}{2}({v_0}^2 - {v_w}^2) - \rho g A_w h_0.$$

With the continuity equation, $Q = A_w v_w = A_0 v_0$, further simplification yields

Table 1
Geometries of common flumes.

Figures	Areas	Wetted perimeters
Rectangular 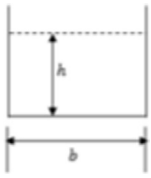	$A = bh$	$P_w = 2h + b$
Trapezoidal 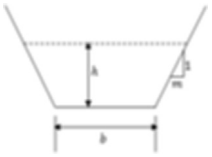	$A = (mh + b)h$	$P_w = 2h\sqrt{1+m^2} + b$
Circular 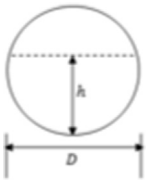	$A = \left(\frac{D}{2}\right)^2 \text{acos}\left(\frac{D-2h}{D}\right) - \left(\frac{D}{2} - h\right)\sqrt{h(D-h)}$	$P_w = D\text{acos}\left(\frac{D-2h}{D}\right)$

$$v_0{}^2 = \frac{2gh_0 - {v_w}^2}{\left(\frac{2A_0}{A_w} sin\theta + 1\right)}. \tag{10}$$

For a known geometry, the flow cross-sectional area as a function of liquid level in the channel is known (see Table 1). Combining the area function $A(h)$ in Table 1 with Eq. (10), the input liquid depth h_0 to the channel for any given flow rate can be calculated.

3. Flow rate measurement models

As mentioned earlier, this paper focuses on formulating an algorithm with improved accuracy for determining the flow rate in open channels based on the hydraulic structure and the slope-hydraulic radius methods. The model applied is specific to any of these methods, and this section gives account of these models for different fluids, geometries and flow conditions.

3.1. Measurement of flow rate using hydraulic structure method

The basic principle underlying the measurement of flow rate in flumes and weirs is the establishment of critical flow condition in the structure [19]. A Flume, as that shown in Fig. 3, usually has a throated section with reduced cross-section, which serves as a control unit for measuring flow rate in the channel. In a well-designed flume, critical

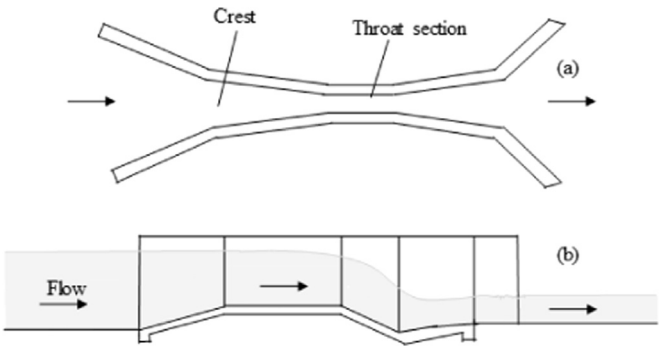

Fig. 3. Top (a) and side (b) views of a Parshall flume.

flow condition always occurs at a point within the throat section for all flow rates in the range of measurement. By considering the specific energy balance between the upstream section and the critical point, the flow rate can be calculated as given in ISO 4359 [20]

$$Q = \left(\frac{2}{3}\right)^{1.5} C_d C_v C_s \sqrt{\frac{g}{\alpha}}\, b_t h_m^{1.5} \tag{11}$$

$$C_v = \left[1 + k\frac{\alpha}{2gh_m}\left(\frac{Q}{A_m}\right)^2\right]^{1.5}.$$

Here, C_d is the coefficient of discharge accounting for losses and C_v is the coefficient correcting the replacement of the specific energy at the measurement point with the measured depth, h_m. C_s is the shape coefficient correcting non-rectangularity of the channel geometry, b_t is the bottom width of the channel at the throat section and A_m is the cross-sectional area of the flow at the point of measurement. α is the average kinetic energy correction factor and k is a dimensionless coefficient introduced in this work to account for the reduced velocity head at the measurement section due to boundary layer effect. Subscript m indicates measured value or evaluated values at measurement point.

In a rectangular cross section, $C_s = 1$ and $k \approx 1.0$, since the effect of boundary layer on the velocity head is small. C_d in a rectangular channel can be obtained from

$$C_d = (1 - 0.006L/b_t)(1 - 0.003L/h_m)^{3/2}. \tag{12}$$

In a trapezoidal channel, the approximate expression for the shape factor and the discharge coefficients are given as follows,

$$C_s = \left[1 + 2\frac{sh_m}{b_t}\right]\left[\frac{1+\frac{sh_m}{b_t}}{1+\frac{5}{3}\frac{sh_m}{b_t}}\right]^{1.5} \tag{13}$$

$$C_d = (1 - 0.006\mu L/b_t)(1 - 0.003L/h_m)^{3/2} \tag{14}$$

$$\mu = \sqrt{1+s^2} - s.$$

Here, s is the side slope of the channel (described as s horizontal to 1 vertical). Due to the sloping side of a trapezoidal channel, the effect of the boundary layer is more significant. Some trial simulations with water show that the value of k is in the order of magnitude of the measured depth, h_m. The geometries of rectangular, trapezoidal and circular channels are given in Table 1. Similar to U-shaped channel, the expressions for C_d and C_s for a circular channel can be found in ISO 4359 [20].

3.2. Measurement of flow rate using slope-hydraulic radius method

Without restricting the flow in an open channel, the flow rate can be computed when the flow is steady and uniform by using the appropriate flow resistance model. When the flow is uniform, the fluid body force due to the channel bed slope is completely absorbed by the frictional resistance to the flow, hence there is no further acceleration of the flow and $S_f = S_0 = \sin\theta$. Based on the resistance models Eqs. (3)–(5) and assuming constant cross-section, the flow rate in an open channel can be obtained from Eq. 15(a - c) for the respective fluid resistance models.

$$Q = \gamma A_m \frac{1}{n_M} {R_{hm}}^{2/3}\sqrt{S_0} \tag{15a}$$

$$Q = \gamma A_m h_m \left(\frac{n}{1+2n}\right)\left(4\frac{\rho g R_{hm}}{K} S_0\right)^{1/n} \tag{15b}$$

$$Q = \gamma A_m R_{hm}\left(\frac{\tau_y}{K}\right)^{\epsilon}\frac{(0.74 + 0.656\epsilon)}{(\epsilon+1)(\epsilon+2)}\left(\frac{\rho g R_{hm}}{\tau_y} S_0 - 1\right)^{\epsilon+0.15} \tag{15c}$$

Here, γ has been introduced as a correction coefficient. The coefficient accounts for uncertainties in the model parameters due to measurement errors, mainly in obtaining the flow resistance characteristic parameters.

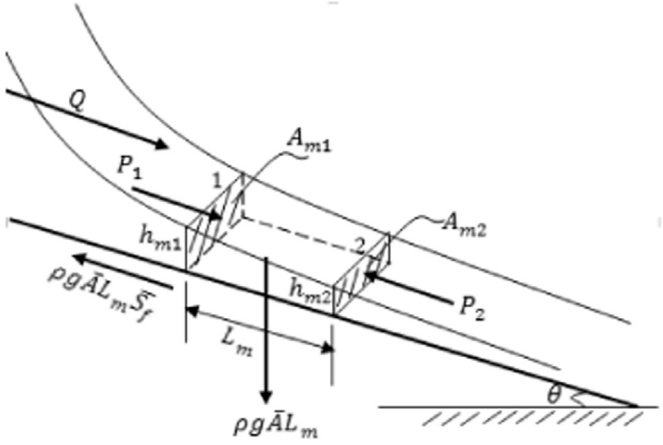

Fig. 4. Free body diagram for accelerating flow in an open channel.

Uniform flow can mainly be achieved in a long channel. However, in many industrial applications the channels are not long enough for a uniform flow to occur in the entire range of desired flow rates. When the flow accelerates the whole length of the channel, the models in Eqs. (15) will overestimate the flow rates. An appropriate model for accelerating flow can be derived based on the momentum balance between any two points in the flow direction. Considering Fig. 4 and neglecting the effect of pressure force, the steady state momentum balance between points 1 and 2 gives

$$\rho Q v_2 - \rho Q v_1 = \rho g \overline{A} L_m \sin\theta - \rho g \overline{A} L_m \overline{S_f}.$$

With $Q = Av$, then

$$Q^2\left(\frac{1}{A_{m2}} - \frac{1}{A_{m1}}\right) = g\overline{A} L_m (S_0 - \overline{S_f})$$

$$Q = \left[\left(\frac{1}{A_{m2}} - \frac{1}{A_{m1}}\right)^{-1} g\overline{A} L_m (S_0 - \overline{S_f})\right]^{1/2}. \tag{16}$$

Here, $\overline{S_f}$ is the average frictional slope obtained from the average velocity and average hydraulic radius of the two points. $\overline{A} = 0.5(A_{m1} + A_{m2})$ is the average cross-sectional area at the two measurement points and L_m is the length of space between the two points. Eq. (16) can be corrected to account for the effect of pressure force and non-uniform distribution of the velocity over each cross-section.

$$Q = C\left[g\overline{A} L_m \left(\frac{1}{A_{m2}} - \frac{1}{A_{m1}}\right)^{-1} (S_0 - \overline{S_f})\right]^{1/2}. \tag{17}$$

In Eq. (17), C is the discharge coefficient, correcting the effect of pressure term and the error associated with the use of average area as the cross-sectional area of the volume bounded by the two points. Dimensional analysis shows that the discharge coefficient depends on the mean hydraulic radius, $\overline{R_h} = 0.5(R_{h1} + R_{h2})$ and L_m, and can be expressed as $C = \left(\frac{L_m}{\overline{R_h}}\right)^{\gamma}$. Eq. (17), thus becomes

$$Q = \left(\frac{L_m}{\overline{R_h}}\right)^{\gamma}\left[g\overline{A} L_m \left(\frac{1}{A_{m2}} - \frac{1}{A_{m1}}\right)^{-1} (S_0 - \overline{S_f})\right]^{1/2}. \tag{18}$$

γ is constant over the entire flow, and some trial simulations performed for a range of flow rates show that $\gamma = 0.01$ could fit the model for a wide range of flow rates. However, in real flow, γ may deviate from the theoretical value. L_m should be reasonably small, but more than the maximum depth of fluid allowed in the channel. The measurement of fluid depth should be taken downstream, at a point no farther than 1/2 of the channel total length from the end.

4. Formulation of estimation algorithm

Since the correction parameters such as α in Eq. (11) and γ in Eqs. (15) and (18), are not known accurately, the accuracy of the models for estimating the flow rate will depend on the chosen value of the correction parameters. In most applications, $\alpha = 1.0$ is used, resulting in the reported measurement accuracy of ± 2–6% [4]. In the slope-hydraulic radius method, the error in using the Manning formula without correction could be up to ± 20%, owing to uncertainty in chosen a value for the Manning's roughness coefficient.

To obtain an improved accuracy in the flow rate measurement using these models, a specific correction parameter should be given to each flow rate, since the real behaviour of a fluid depends largely on its flow rate. In this section, an algorithm for improving on the accuracy of flow rate estimation is proposed. The method developed here involves comparing the simulated fluid depths at the measurement points with the actual depths measured. The resulting error is used to calibrate the flow rate model by adjusting the appropriate correction parameter. Considering Eq. (11), it follows that

$$Q \propto \frac{C_v}{\sqrt{\alpha}},$$

where $\frac{C_v}{\sqrt{\alpha}} = \frac{1}{\alpha^{\frac{1}{2}}}\left[1 + k\frac{\alpha}{2gh_m}\left(\frac{Q}{A_m}\right)^2\right]^{\frac{3}{2}}$, which on further expansion gives

$$\frac{C_v}{\sqrt{\alpha}} = (\alpha^{-1} + 3\Phi + 3\Phi^2\alpha + \Phi^3\alpha^2)^{1/2},$$

where $\Phi = \frac{k}{2gh_m}\left(\frac{Q}{A_m}\right)^2$.

Since in subcritical flow condition, the Froude number, $Fr = \frac{\left(\frac{Q}{A_m}\right)}{\sqrt{gh_m}} < 1$, the higher order terms in Φ are insignificant in the expression above, resulting in

$$\frac{C_v}{\sqrt{\alpha}} \approx (\alpha^{-1} + 3\Phi)^{1/2}. \tag{19}$$

Eq. (19) shows that increasing α will decrease the flow rate, and decreasing it will increase the flow rate. This means that when larger value of α than necessary is chosen, Q will be *underestimated*, while Q will be *overestimated* with a much lower value of α. The depth of fluid in the channel increases with the flow rate. When the simulated liquid depths are higher than the actual liquid depths, the focus will be to reduce the estimated flow rate. Reducing Q requires increasing α. Supposing α_0 is the initial guess of α, the correct estimation of Q will be obtained by adjusting α iteratively based on the following conditions

$$\alpha = \begin{cases} \alpha_0 - \delta\alpha; & if\ h_m > h_{ms} \\ \alpha_0 + \delta\alpha; & otherwise \end{cases}, \tag{20}$$

where $\delta\alpha$ is an offset of previously determined value of α, which can be set as $\delta\alpha = 0.01$ since the sensitivity of the model to α is quite significant, and h_{ms} is the simulated liquid depth at the measurement point.

In Eq. (15), Q is directly proportional to γ, and in Eq. (18), Q also increases with γ since the ratio $\frac{L_m}{\bar{R}_h} > 1$. In using the slope-hydraulic-radius method, Q is correctly estimated by adjusting γ iteratively based on the following conditions

$$\gamma = \begin{cases} \gamma_0 - \delta\gamma; & if\ \bar{h}_m < \bar{h}_{ms} \\ \gamma_0 + \delta\gamma; & otherwise \end{cases}, \tag{21}$$

where $\bar{h}_m$ and $\bar{h}_{ms}$ are the average of the two actual measured liquid depths, and the simulated liquid depths, respectively. Since the sensitivity of the models to γ is not too significant within the model accuracy, the offset $\delta\gamma$ can be set as 0.05 for models in Eq. (15) and as 0.005 for that in Eq. (18).

In the slope-hydraulic radius method, both models, Eqs. (15) and (18) are used concurrently for continuous measurement of flow rate. This is because for a low flow rate, there is possibility that the flow will reach a uniform state before discharging the channel while with a high flow rate, the flow may not attain uniform state within the channel length. Incorporating both models in the estimation algorithm ensures a wide range of flow rate estimation. In Eq. (15), the measured fluid depth used for computation is the average value of h_{m1} and h_{m2}. Switching between uniform and accelerating flow models depends on the measured liquid depth difference, $\Delta h_m = h_{m1} - h_{m2}$ and on the computed effective slope, $S_e = S_0 - \bar{S}_f$. The following gives the general switching condition, where $Im(S_e)$ = Imaginary part of S_e.

$$Q = \begin{cases} Eq.\ (15); & if\ \Delta h_m < 10^{-4}\ m\ or\ Im(S_e) \neq 0 \\ Eq.(18); & otherwise \end{cases}$$

For a given channel geometry, bed slope and fluid properties, the algorithm for computing the flow rate in the channel based on the slope-hydraulic radius and on the use of Venturi channel is summarized in the following sections.

4.1. Venturi model

1. Read level h_m.
2. With α_0, compute $Q^{(0)}$ from Eq. (11).
3. With $Q^{(0)}$, solve Saint Venant equations to give $h_{ms}^{(0)}$. Let $i = 0$.
4. Repeat until $|h_{ms}^{(i)} - h_m| \leq 10^{-5}$.
5. Set $\alpha_i \rightarrow \alpha_{i+1}$, applying Eq. (20).
6. Recompute $Q^{(i+1)}$ from Eq. (11).
7. Resolve Saint Venant equations using $Q^{(i+1)}$, leading to $h_{ms}^{(i+1)}$.
8. Set $i \rightarrow i + 1$, and go to 4.
9. Write $Q = Q^{(i)}$.

4.2. Slope-hydraulic radius model

1. Read levels h_{m1} and h_{m2}.
2. With γ_0, compute $Q^{(0)}$ from Eqs. (15) or (18).
3. With $Q^{(0)}$, solve Saint Venant equations to give $h_{ms1}^{(0)}$ and $h_{ms2}^{(0)}$. Let $i = 0$.
4. Repeat until $|\bar{h}_{ms}^{(i)} - \bar{h}_m| \leq 10^{-5}$.
5. Set $\gamma_i \rightarrow \gamma_{i+1}$, applying Eq. (21).
6. Recompute $Q^{(i+1)}$ from Eqs. (15) or (18).
7. Resolve Saint Venant equations using $Q^{(i+1)}$, leading to $h_{ms1}^{(i+1)}$ and $h_{ms2}^{(i+1)}$.
8. Set $i \rightarrow i + 1$, and go to 4.
9. Write $Q = Q^{(i)}$.

Fig. 5 illustrates the above algorithms in block form for flow rate computation. The dotted line surrounding the calculation blocks indicates the iteration loop for updating the tuning parameter such as α used in the hydraulic structure method or γ used in the slope-hydraulic radius method. When implementing the algorithm in software, Fig. 5 shows the exact arrangement, with a clear correspondence between graphical symbol and section of code. The algorithm can easily be implemented in MATLAB. The set of ordinary differential equations (ode) for simulating the flow can be solved using a MATLAB ode solver.

5. Results and discussion

In this section, the results obtained with the developed algorithm are presented. Two cases are considered: one comparing the computed flow rates with experimental data for a steady state flow in a Venturi channel, and the other demonstrating the performance of the scheme in unsteady state flow.

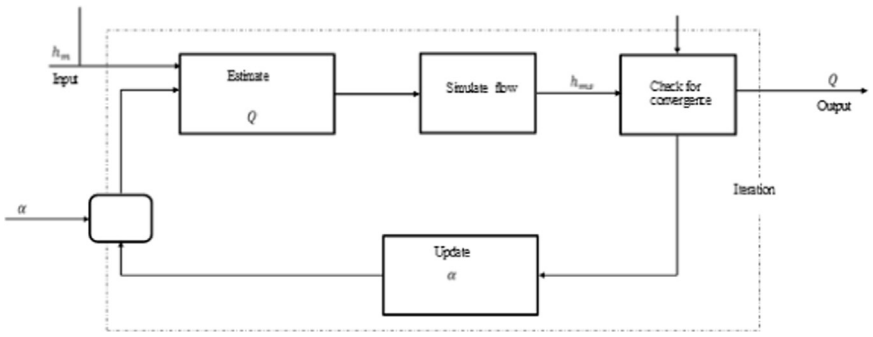

Fig. 5. Block diagram for implementation of the algorithm for flow rate estimation.

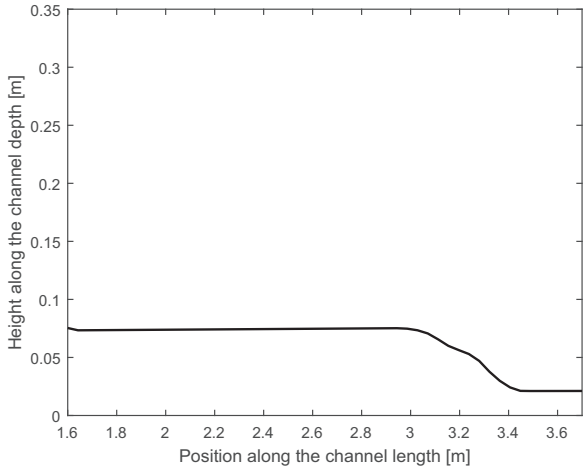

Fig. 6. Simulated depth of the mud flow along the trapezoidal Venturi channel.

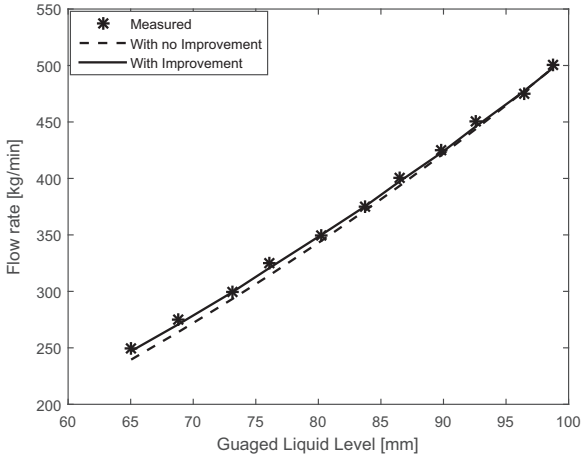

Fig. 7. Computed versus measured flow rates in the Venturi channel.

5.1. Flow rates in steady state flows

At University College of Southeast Norway, a Venturi channel test rig has been set up. The channel is of trapezoidal cross-section with a total length of 3.70 m. The detailed description of the rig can be found in Agu et al. [15].

Fig. 6 shows the steady state flow profile in the channel at flow rate 350 kg/min, simulated for a slurry with density, 1109 kg/m^3, and rheological parameters, $\tau_y = 0$, n = 0.5855 and K = 0.0631 Pa.s^n. The channel is inclined at 0.08°. From Fig. 6, it can be seen that the flow accelerates from the converging section, and further through the throat section (within a distance of 3.1 and 3.3 m from the leading end). The flow discharges freely at supercritical condition.

Fig. 7 compares the measured flow rate with the computed flow rates based on single depth measurement taken at a point 2.6 m from the leading end, and applying Eq. (11). The results (data marked "With Improvement") show that the algorithm developed in this paper yields an improved accuracy when compared with the traditional method where $\alpha = 1.0$ (data marked "With no Improvement"). The error associated with the computed flow rate with $\alpha = 1.0$ is 2.33%. The error is calculated based on the relative error given by $\sqrt{\frac{1}{N}\sum\left(\frac{Q_{exi} - Q_{si}}{Q_{exi}}\right)^2}$, where N is the number of data points, Q_{exi} and Q_{esi} are the individual measured and computed flow rates in the data set, respectively. Using the improvement algorithm, the error is reduced to 0.83%, corresponding to an improvement of about 64%. The computation time for each flow rate based on the improved scheme takes about 2 s of computer time, which can be reduced with more efficient code and higher speed computers.

5.2. Flow rates in dynamic flows

In the second case, the return of flow from a well over a circular channel is simulated. The 8.432 m long channel with a diameter of 0.4064 m (16 in.) is inclined at 7° with the horizon. The well is an annulus, with core and outer diameters, 0.1397 m (5.5 in.) and 0.5334 m (21 in.), respectively. The noisy flow variation of a fluid through the well and then through the straight run channel over 10 min is given by the function depicted in Fig. 8.

Assuming a fluid with density 1400 kg/m3, and rheological parameters: $\tau_y = 2.21$ Pa, $n = 0.7703$ and $K = 0.2$ Pa.s^n, Fig. 9 gives the fluid depth profile in the channel at instances 15, 30, 225 and 450 s of the flow. The flow is supercritical over the length of the channel at all instances. The supercritical flow behaviour in the channel is due to steep slope of the channel (bed slope of 7°). It can be seen from the result that at the instances when the flow rate is high, the flow accelerates down the channel, but at the low flow rates (at instances 15 and 30 s for example), the flow seems to have reached uniform flow condition

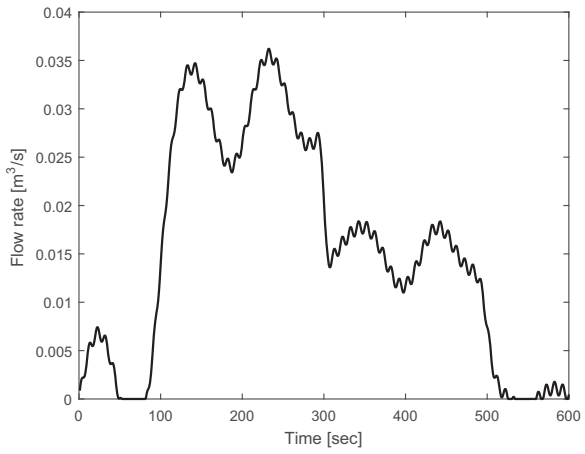

Fig. 8. Variation of drilling fluid flow rate in a well over a period of 10 min.

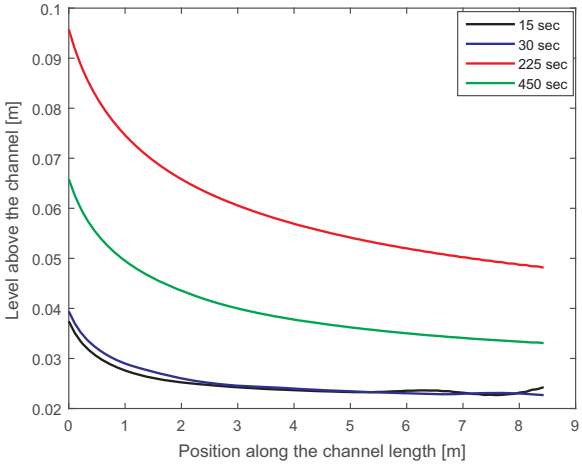

Fig. 9. Instantaneous liquid depth profiles of the drilling fluid in the circular channel.

before leaving the channel. To estimate the flow rate in the channel, as described in Section 3.2, two simulated liquid depths are required. The simulated liquid depths are taken at 1-s interval.

Fig. 10 shows the evolution of simulated liquid depths h_{s1} taken at $x = 4.637$m and h_{s2} taken at $x = 4.848$ m from the leading upstream end, with time. The lower plot of Fig. 10 shows that there is a significant difference between these two depths within the flow interval 100 and 500 s (that is the difference in the depths is above 10^{-4} m). Within this period, the flow rate is high as can be seen in Fig. 8. In the rest of the flow period, the depth difference is mixed (that is partly greater and partly less than 10^{-4} m). This variation in the two depths suggests that both the uniform and accelerated models will be required to compute the flow rate in the entire flow duration.

By using the switching algorithm developed here, Fig. 11 compares the results of the computed flow rates with the input flow rate over the flow duration. The result shows a good agreement between the computed and the given flow rate. It also shows that despite the dynamics of the system (where it is possible that the flow has not been developed before taking the measurements), the algorithm is able to compute the flow rate with small error. The deviations of the computed flow rate from the actual are shown in Fig. 12, where it can be seen that the computation error lies between -0.005 and $0.003\ \mathrm{m}^3/\mathrm{s}$. The analysis of the error (based on $\frac{\sqrt{\frac{1}{N}\sum(Q_{exi}-Q_{si})^2}}{\frac{1}{N}\sum Q_{exi}}$ for the accumulated flow over the entire flow duration) shows that the deviation is less than 5.64%. Most of the errors are associated with computation of flow rates less than $5 \times 10^{-5}\ \mathrm{m}^3/\mathrm{s}$, due to difficulty in simulating such a low flow rate in the channel.

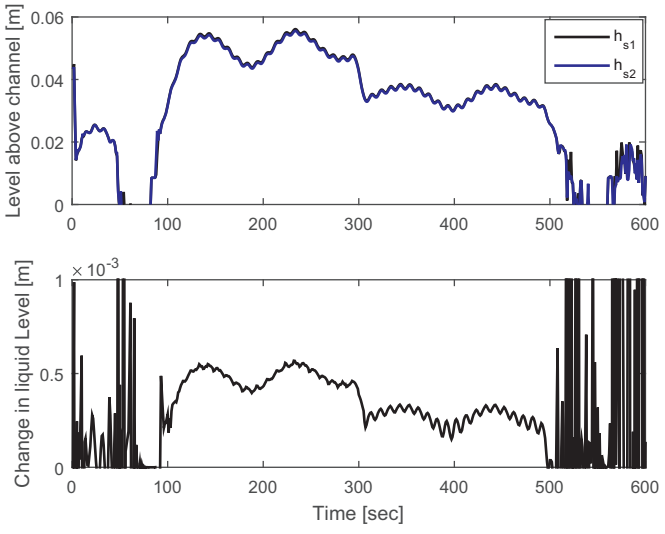

Fig. 10. Evolution of the simulated liquid levels at the gauged points (upper plot) and their difference (lower plot) with time.

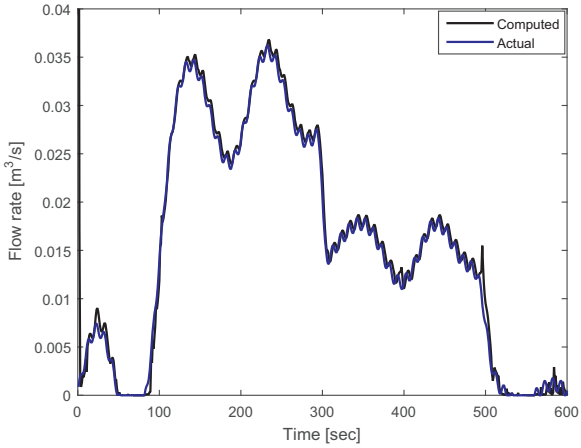

Fig. 11. The computed versus the actual flow rates in the circular channel.

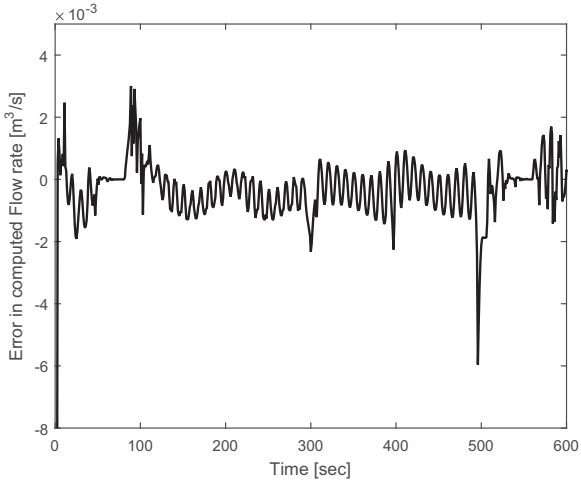

Fig. 12. Evolution of computed flow rate errors in the circular channel.

6. Conclusions

In this paper, an algorithm for improving on the accuracy of flow rate computation in open channels is proposed. The study covers two flow rate computational methods: hydraulic structure, mainly with flumes, and the slope-hydraulic radius method. In addition to the flow resistance model, which is usually applied in the slope-hydraulic radius method for uniform flow, a model for computing the flow rate in an accelerating flow is developed.

The results show that the proposed algorithm leads to improvement in the accuracy of flow rate calculations based on the hydraulic structure by 65% under experimental verification. For the case studied with a trapezoidal channel, the computation error is reduced from 2.33% to 0.83%. The computation of flow rate in a straight-run channel under dynamic condition is theoretical verified, and the result shows that the switching algorithm between a uniform and an accelerated flow models can estimate the flow rate with small error irrespective of whether the flow is fully developed or not within the measurement interval. With the computation time less than 2 s, this shows that the proposed algorithm is also efficient, and with some improvement, it could be used for continuous flow rate computation required for control purposes.

The proposed algorithm has been demonstrated for systems within

industrial scale. For large systems such as river flooding, the algorithm requires further verification. Moreover, the experimental verification of the proposed algorithm for slope-hydraulic radius method will be considered in the future work.

Acknowledgement

The funding from Statoil ASA and the support from its Intelligent Drilling group, are gratefully acknowledged.

References

[1] N.J. Balmforth, R.V. Craster, Geophysical Aspects of Non-Newtonian Fluid Mechanics, LNP, 582 Springer, Berlin, 2001, pp. 34–51.
[2] J.D. Bankston, F.E. Baker, Open channel flow in aquaculture, Southern Regional Aquaculture Centre, 374 SRAC publication, 1995.
[3] OpenChannelFlow, Methods of measuring flows in open channel. 〈http://www.openchannelflow.com/blog/methods-of-measuring-flows-in-open-channels〉 (Accessed 27 February 2017).
[4] A.J. Clemens, T.L. Wahl, M.G. Bos, J.A. Replogle, Water Measurement with Flumes and Weirs, Publication 58, International Institute for Land Reclamation and Improvement, The Netherlands, 2001.
[5] K.C. Wilson, Flume design for homogeneous slurry flow, Part. Sci. Technol. (1991) 149–159.
[6] F.A. Kilpatrick, V.R. Schneider, Use of Flumes in Measuring Discharge, Techniques of Water Resources Investigations of the United States Geological Survey (Book 3, Ch. AI4), USGS, Boulder, 1983, p. 46.
[7] R.E. Smith, D.L. Chery, Jr. K.G. Renard, W.R. Gwinn, Supercritical flow flumes for measuring sediment-laden flow, Department of Agriculture Technical, Bulletin No. 1655, Illus, U.S, p. 72.
[8] C.I. Thornton, B.A. Smith, S.R. Abt, M.D. Robeson, Supercritical flow measurement using a small Parshall flume, J. Irrig. Drain. Eng. 135 (2009) 683–692.
[9] W. Boiten, Flow measurement structures, Flow Meas. Instrum. 13 (2002) 203–207.
[10] H. Yeung, An examination of BS3680 4C (ISO/dis 4369) on the measurement of liquid flow in open channels – flumes, Flow Meas. Instrum. 18 (2007) 175–182.
[11] C. Berg, A. Malagalage, C.E. Agu, G.-O. Kaasa, K. Vaagsaether, B. Lie, Model-based drilling fluid flow rate estimation using Venturi flume, IFAC-Pap. 48 (6) (2015) 171–176.
[12] E.A. Meselhe, F. Sotiropoulos, F.M. Holly-Jr, Numerical simulation of transcritical flow in open channel, J. Hydraul. Eng. 123 (1997) 0774–0783.
[13] C. Sart, J.-P. Baume, P.-O. Malaterre, V. Guinot, Adaptation of Preissmann's scheme for transcritical open channel flows, J. Hydraul. Res. 48 (2010) 428–440.
[14] G.S. Stelling, S.P.A. Duinmeijer, A staggered conservative scheme for every Froude number in rapidly varied shallow water flows, Int. J. Numer. Methods Fluids 43 (2003) 1329–1354.
[15] C.E. Agu, G. Elseth, B. Lie, Simulation of transcritical flows in hydraulic structures, in: Proceedings of the 56th Conference on Simulation and Modelling, Linköping, Sweden, 2015.
[16] R. Szymkiewicz, Numerical Modeling in Open Channel Hydraulics, 83 Springer, 978-90-481-3673- 5, 2010.
[17] R. Sisson, P. Lacoste-Bouchet, M. Vera, M. Costello, E. Hedblom, B. Sheets, L. Sittoni, An Analytical model for tailings deposition from pilot-scale testing, in Proceedings of the 3rd International Oil Sand Tailings Conference, Edmonton, Canada, 2012.
[18] M. Jin, D.L. Fread, One-dimensional routing of mud/debris flows using NWS FLDWAV model, in: Chenlung Chen (Ed.), Debris-Flow Hazards Mitigation: Mechanics, Prediction, and Assessment, ASCE, New York, 1997, pp. 687–696.
[19] Ministere du Developpment durable, de L'environment et Desparcs du Que'bec, Sampling Guide for Environmental Anlysis: Booklet 7 - Flow Measurement Methods in Open channels, Centre d'expertiseen analyse environmentale du Que'bec, p. 223.
[20] ISO 4359, Flow Measurement Structures – Rectangular, Trapezoidal and U-shaped Flumes, International Standard, Switzerland, 2013.